May 9-12
Kyoto-Japan
2017

2nd International Workshop on
Sediment Bypass Tunnels

Hydraulics of water, air-water and sediment flow in downstream-controlled sediment bypass tunnels

Robert M. Boes, Claudia Beck, Nicola Lutz, Adriano Lais and Ismail Albayrak

Abstract

While most sediment bypass tunnels (SBTs) are gate-controlled at the intake, so that the flow regime downstream of the gate is free-surface, some SBTs are controlled at their downstream end, e.g. due to spatial restrictions hindering the arrangement of the gate at the intake. For downstream control, the flow regime may change from free-surface via transitional to pressurized, mainly depending on the gate opening, the bed slope and the available head at the intake. Because the flow regime has a considerable effect both on the sediment transport and the transport of air being potentially entrained at the intake, the hydraulic design is crucial for the safe and reliable operation of SBTs. A poor design may have severe consequences such as pressure fluctuations, air blow-up, gate vibrations and cavitation erosion, thus compromising the structural safety.

This paper deals with the hydraulic model investigation of the rectilinear Patrind SBT, Pakistan, conducted at the Laboratory of Hydraulics, Hydrology and Glaciology (VAW) of ETH Zurich, Switzerland. The SBT has the following key features (referring to the optimized design): downstream-control by a tainter gate, length of 181.5 m, archway section over length of 140.5 m with b x h = 7.5 x 8.5 m and maximum discharge capacity of some 900 m^3/s at full supply level. The main foci of the present study are on problems with air entrainment, transport and detrainment as well as on sediment transport for downstream-controlled SBTs. Mitigation measures such as the placement of detrainment devices are discussed.

Keywords: flow regime, air transport, sediment transport, de-aeration device, incipient cavitation

1 General layout of SBT

A typical SBT layout includes a tainter or slide gate as regulating device at the inlet, followed by a mostly short and steep flow accelerating section and a more gently sloped standard cross section until the outlet with subsequent energy dissipating structure such as free-falling jet and plunge pool (Fig. 1). Supercritical flow regime is preferred in SBTs to limit the tunnel dimensions, to increase bedload transport capacity and to avoid

sediment deposition in the tunnel. Therefore, in most SBT the flow is accelerated at the inlet either by pressurized flow upstream of the gate (in case of submerged SBT intakes, Auel and Boes 2011) or by a steep section downstream (d/s) of the gate (Fig. 1) to quickly reach quasi-uniform supercritical flow. Free-surface flow is preferred, but pressurized flow for the design discharge may also occur, depending on the location of the gates that determine the control section. Some SBT like Patrind, Pakistan (Beck *et al.* 2016), and Rizzanese, France (Carlioz and Peloutier 2014, Laperrousaz and Carlioz 2015), are d/s gate-controlled, mostly due to site constraints disabling a gate installation at the inlet. In the latter cases, free-surface flow, transitional flow and pressurized flow may occur, depending on the discharge.

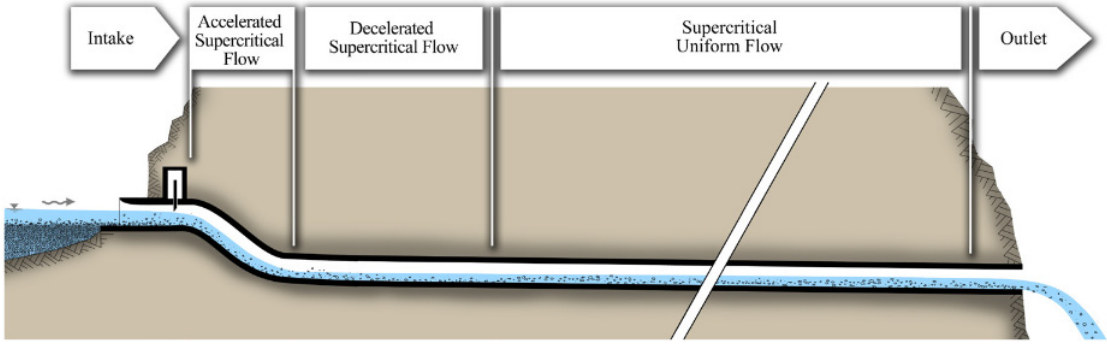

Fig. 1: Typical longitudinal section of an upstream-controlled SBT (Auel 2014).

Regarding flow velocities, there is a trade-off between the risk of aggradation (favouring flow choking and clogging) and the target to keep velocities moderate. While flow velocities must be sufficiently high to avoid sediment deposition, the maximum velocities should be as small as possible to minimize bed shear stresses and to control the extent of invert abrasion (Hagmann *et al.* 2016).

2 HPP Patrind layout

2.1 Project overview

The Patrind hydropower project (Patrind HPP) features a dam site on the Kunhar River in Pakistan 120 km northeast of Islamabad creating an initial storage capacity of around 6 Mio. m^3. A cofferdam (Fig. 2, ⑥) was built about 300 m upstream (u/s) of the dam for the river diversion during construction, creating a settling basin between the cofferdam and the gravity dam (Fig. 2, ⑤). U/s of the cofferdam with crest elevation at 755.0 m a.s.l., an approx. 181.5 m long SBT (Fig. 2, ⑦) was constructed to divert floods with high sediment loads and additionally to convey sediments to the d/s river reach during drawdown flushing. The scheme featuring a settling basin for trapping fine sediment and an SBT for diverting bedload as well as suspended sediments is referred to as “re-arranged sandtrap” or “natural desander” (Alam *et al.* 2015). The goal of the concept is to remove grains larger than $d = 0.2$ mm from the water entering the power intake (Fig. 2, ③) and

headrace tunnel (Fig. 2, ④) while maintaining the long-term reservoir storage capacity. The HPP design discharge is $Q_{d,HPP}$ =154 m^3/s, and the settling basin is operated between the full supply level (FSL) at 765 m a.s.l. and a minimum operation level (MOL) of 760 m a.s.l. up to a 5-year flood. During floods, the reservoir is drawn down using the dam spillways (Fig. 2, ①, ②) and the SBT. As the drawdown might not be complete, especially for large floods, the water level during this operation might still be quite high, resulting in rather low bed shear stresses. Previous bed load aggradations in the reservoir will therefore not be remobilized, so that an additional annual flushing with low discharges and free-flow conditions in the SBT will still be necessary to flush out sediments from both the settling basin and the reservoir u/s of the cofferdam (Beck *et al.* 2016). All bedload from the main reservoir is thereby flushed through the SBT. The characteristic hydrologic flood peaks from the catchment with an area of 2,400 km^2 are estimated as follows: annual flood 342 m^3/s, 5-year flood 815 m^3/s, 10-year flood 1,037 m^3/s, 100-year flood 2,026 m^3/s, 350-year flood (design flood) 2,799 m^3/s, and probable maximum flood (PMF) 4,061 m^3/s.

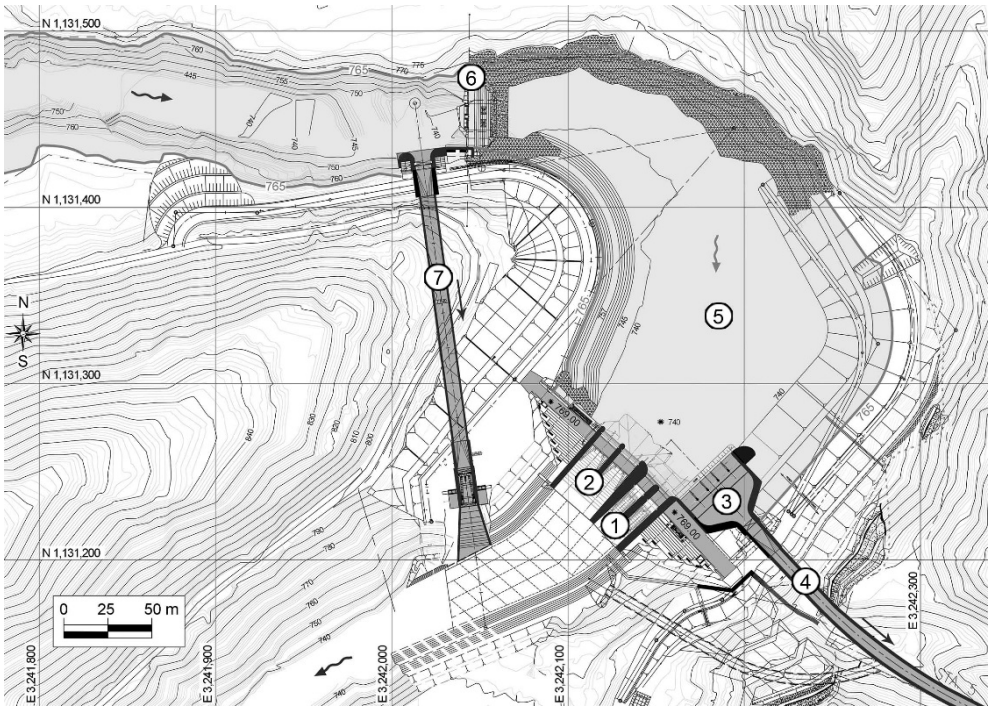

Fig. 2: Plan view of the Patrind HPP dam site featuring the underflow spillways ①, the overflow spillways ②, the power intake ③, the headrace tunnel ④, the natural settling basin ⑤, the cofferdam ⑥ and the sediment bypass tunnel ⑦ (from Beck *et al.* 2016).

2.2 SBT layout

The inlet structure of the SBT is situated 30 m u/s of the cofferdam in the right valley flank. A maintenance slide gate in the SBT inlet structure is housed in a hoist tower slightly protruding into the reservoir cross section. Three air vents of 0.1 m diameter are

situated directly d/s of this slide gate at the start of the profile transition from rectangular to archway (Fig. 3).

The tunnel with an archway profile 8.5 m high and 7.5 m wide (cross-sectional area 57.7 m^2) has a concrete lining with a compressive strength of 60 MPa, a slab thickness of 1.2 m and connects the u/s reservoir with the d/s river reach. The tunnel discharge is regulated by a radial gate with a radius of 14 m at the end of the SBT. The SBT outlet structure is situated at the end of the stilling basin of the dam spillways in the right valley flank (Fig. 2). The SBT outlet chute is conically shaped in longitudinal profile with an angle of expansion of 9.7° in plan view. The SBT bed slope of 1.12% is constant between the end of the rectangular inlet cross section and the beginning of the conical outlet chute d/s of the radial gate (Fig. 3).

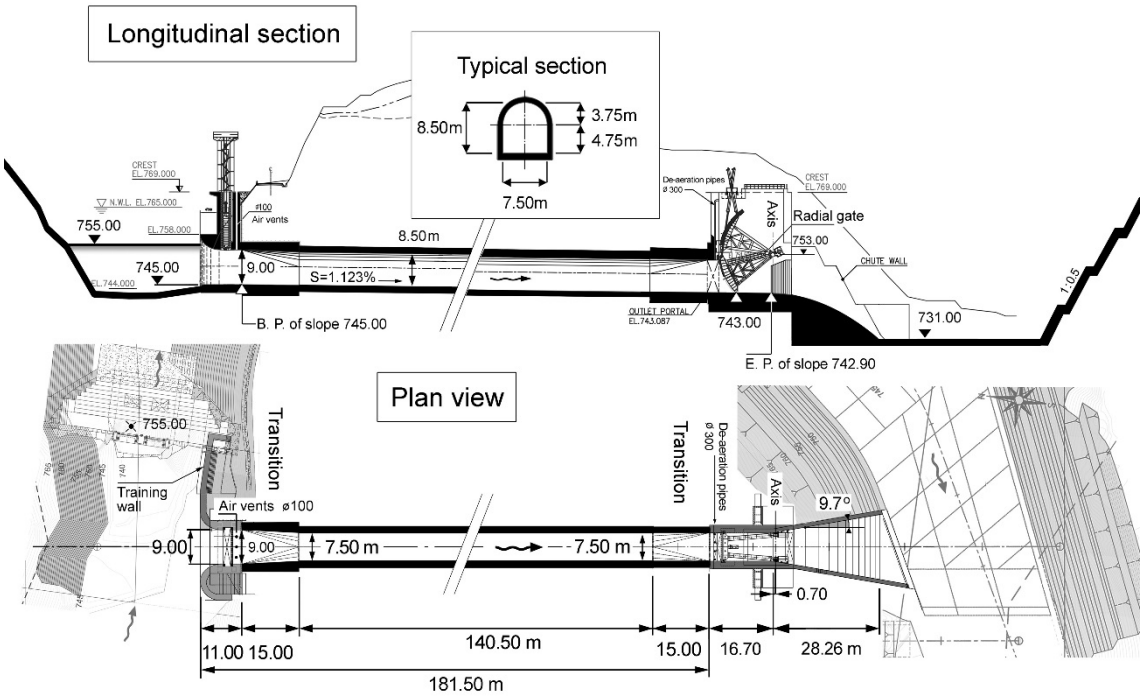

Fig. 3: Longitudinal section (top) and plan view (bottom) of the final Patrind SBT design (from Beck *et al.* 2016).

3 SBT Patrind flow conditions

3.1 Operation regimes and flow conditions

The discharge capacity for fully-opened gate vs. the reservoir head H_R is illustrated in Fig. 4, from which the free-surface flow, transition flow and pressurized flow regimes can be depicted.

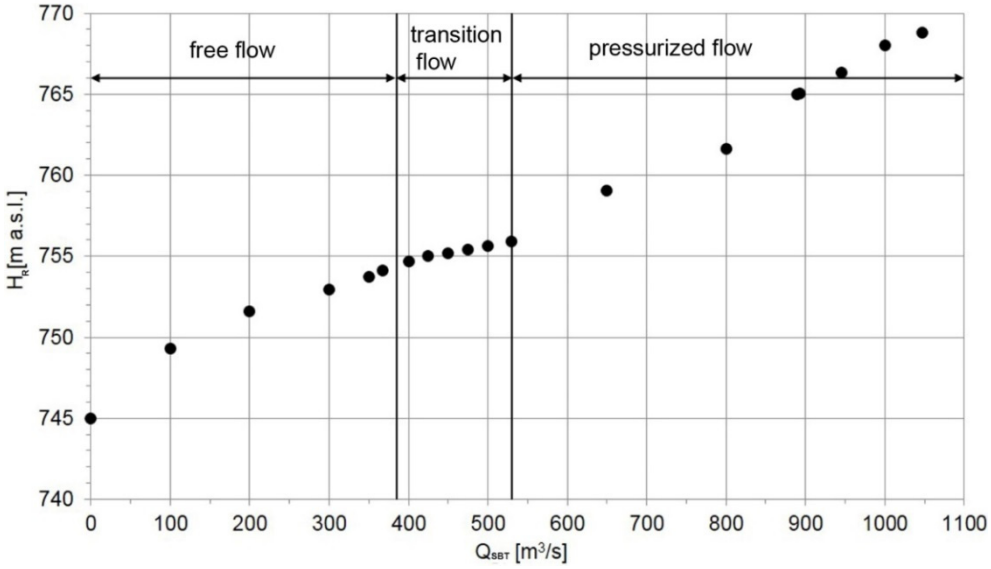

Fig. 4: SBT discharge Q_{SBT} versus reservoir level H with fully-opened gate; the range of transition flow is indicated (adapted from VAW 2016).

The following flow regimes are observed for **completely opened radial gate** depending on the reservoir level H_R:

1) $\boldsymbol{H_R \leq 754.5}$ **m a.s.l.** ($Q_{SBT} \leq 385$ m^3/s):

- Free-surface flow, free air circulation in the SBT (Fig. 5a).
- Relevant for flushing or for the receding limb of a flood hydrograph.

2) **754.5 m a.s.l.** $< \boldsymbol{H_R} \leq$ **755.2 m a.s.l.** (385 m^3/s $< Q_{SBT} \leq 450$ m^3/s):

- Transition from free-surface to pressurized flow starting from the inlet section. Only the inlet portion down to the break point (B.P.) of slope is under pressurized flow, the air vents d/s of the inlet slide gate being submerged (Fig. 5b).
- Relevant during drawdown flushing or during a flood event with a peak discharge up to 450 m^3/s.

3) **755.2 m a.s.l.** $< \boldsymbol{H_R} \leq$ **755.9 m a.s.l.** (450 m^3/s $< Q_{SBT} \leq 530$ m^3/s):

- Transient flow conditions, accumulation and transport of large air pockets along the SBT roof (elongated bubble flow, Fig. 6).
- Relevant for drawdown flushing during small flood events.

4) $\boldsymbol{H_R >}$ **755.9 m a.s.l.** ($Q_{SBT} > 530$ m^3/s):

- Full filling of the SBT, pressurized flow, air entrainment due to intake vortices (see section 4.1) in case of no discharge towards the cofferdam and through dam spillways, negative pressures act on the tunnel roof.

- Not relevant for the project in case of flushing during flood events because no air-entraining vortices develop with flow towards the cofferdam.

The following flow features were detected in the physical scale model for the diversion of small floods through the SBT during power operation (Q_{SBT} = 100-650 m^3/s, Q_{HPP} = 154 m^3/s). The reservoir level is thereby sustained by regulating the SBT gate at **partial gate openings**:

5) ***H_R* = 760-765 m a.s.l., power operation, partial gate opening**

- Pressurized flow regime, air entrainment due to intake vortices (see section 4.1).
- Relevant for all load cases with power operation, where an excess discharge of Q_{SBT} > 100 m^3/s is diverted through the SBT.

3.2 Free-surface flow conditions

For free-surface flow conditions, which occur for fully opened gate and discharges $Q_{SBT} \leq$ 385 m^3/s, the flow is controlled by the hydraulic capacity of the critical flow section where the critical flow depth h_c and the critical flow velocity v_c are reached. The critical flow section is located at the end of the transition zone (x = 15 m, Fig. 3). D/s from that, the flow changes to supercritical flow and continuously accelerates (drawdown curve, Fig. 5a). Towards the d/s end of the tunnel at station x = 155.5 m approx. 105-115% of the uniform flow depth h_u are reached, i.e. the SBT is too short for the development of uniform flow.

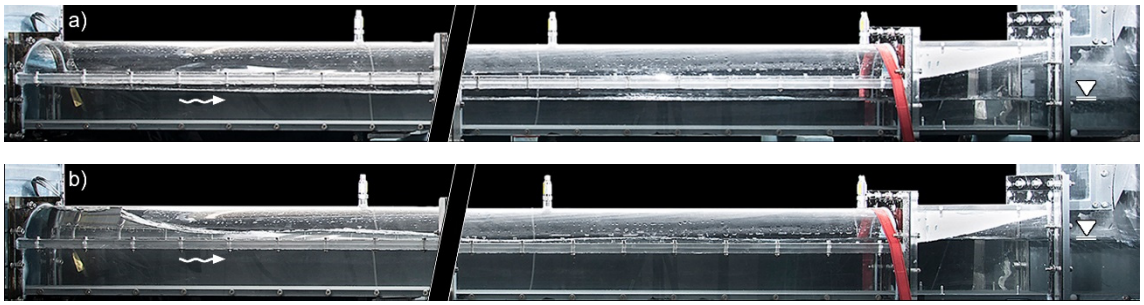

Fig. 5: SBT side view during free-flow conditions for a discharge of Q_{SBT} = a) 200 m^3/s and b) 400 m^3/s with a submerged inlet structure. The SBT outlet gate is fully opened (adapted from VAW 2016).

3.3 Transition flow

If the reservoir level exceeds 754.5 m a.s.l. at fully opened gate, the SBT inlet section with a roof level of 754 m a.s.l. submerges, while in the d/s part of the SBT free-flow conditions prevail (Fig. 5b).

With increasing reservoir level and SBT discharge, e.g. at Q_{SBT} = 450 m^3/s, a transient process is observed (H_R = 755.2 m a.s.l.). The transient process begins with a submerged inlet portion and free flow in the d/s part of the tunnel (compare Fig. 5 with Fig. 6a). The level of the pressure line falls below the tunnel roof according to the energy conservation

law. Negative pressures act on the tunnel roof right after the transition zone where full filling prevails. Due to the small intake submergence of 1.2 m, air is pulled in through the inlet structure (Fig. 6b). The air bubbles are transported d/s and cause pronounced pressure fluctuations and transition to elongated bubble flow regime (Fig. 6c). Once the air pockets collide they merge to one single bubble (Fig. 6d), resulting in a blowout of pressurized flow (free flow prevails in the d/s part of the tunnel) and the transient process starts with filling of the upper tunnel part again (Fig. 6a). In the outlet section, free-surface flow is observed during tunnel transition flow.

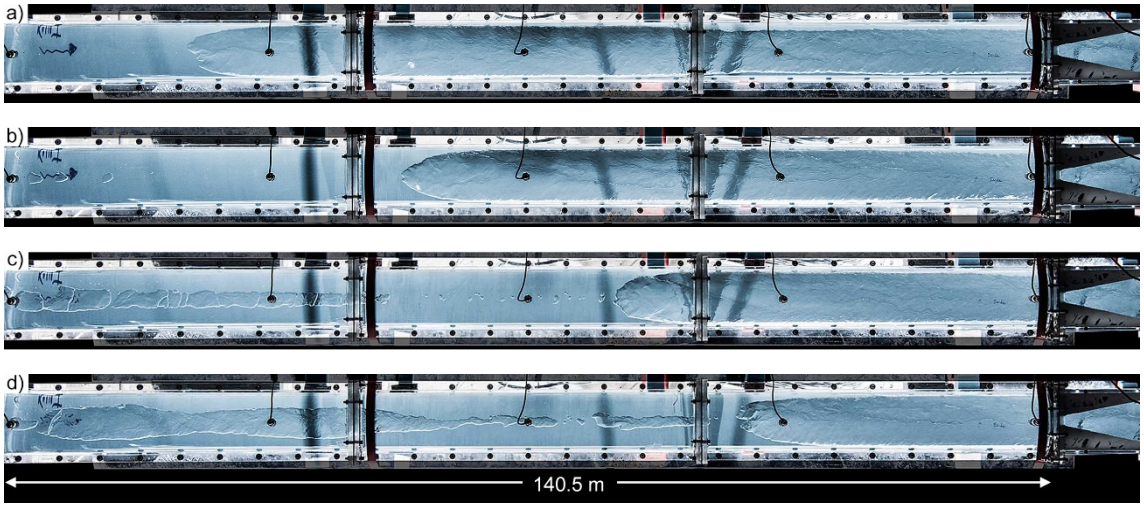

Fig. 6: Top view of the SBT during transition flow for Q_{SBT} = 450 m^3/s and fully-opened radial gate with negative pressure acting on the tunnel roof: a) The flow chokes the inlet and the u/s portion while free-surface flow prevails along the d/s tunnel; b) the tunnel gets pressurized in flow direction and air is supplied in the u/s reach; c) the flow regime changes to elongated bubble flow; d) once the elongated bubbles aggregate to one single bubble the pressurized flow is blown out and stratified flow develops. The transient process starts with a) again (adapted from VAW 2016).

In the transition flow regime, the entrapped air is transported along the tunnel roof as elongated bubbles. At the end of the pressurized tunnel portion, the large air bubbles discharge unhindered to the free atmosphere and cause a pressure gradient between the u/s and d/s bubble end (section 4.2). This leads to an acceleration of the following water front and oscillations of the upper jet trajectory and consequently to pressure fluctuations on the SBT outlet lining. However, such pressure fluctuations are generally small compared to the strain at high reservoir levels and therefore not crucial for the safety of the structure. Nevertheless, the alternating strain and the corresponding fatigue strain have to be considered.

To get an impression on the pressure fluctuations acting on the SBT roof lining during transition flow, pressure measurements in the middle of the tunnel for Q_{SBT} = 500 m^3/s are shown in Fig. 7. Due to the transition flow and the transport of air bubbles, the acting pressures include a certain periodic load. A peak-to peak pressure amplitude of about 2.5 m w.c. and dynamic pressure coefficients of $C_p' = h_p'/(h_{p,mean} + v^2/2g) = 0.12$ result

during pressurized flow, where $h_{p,mean}$ and h_p' denote the mean measured pressure head and the pressure fluctuations (standard deviation), respectively, and v = cross-sectional averaged flow velocity. Note the negative pressure heads during phases of full filling of the tunnel in Fig. 7.

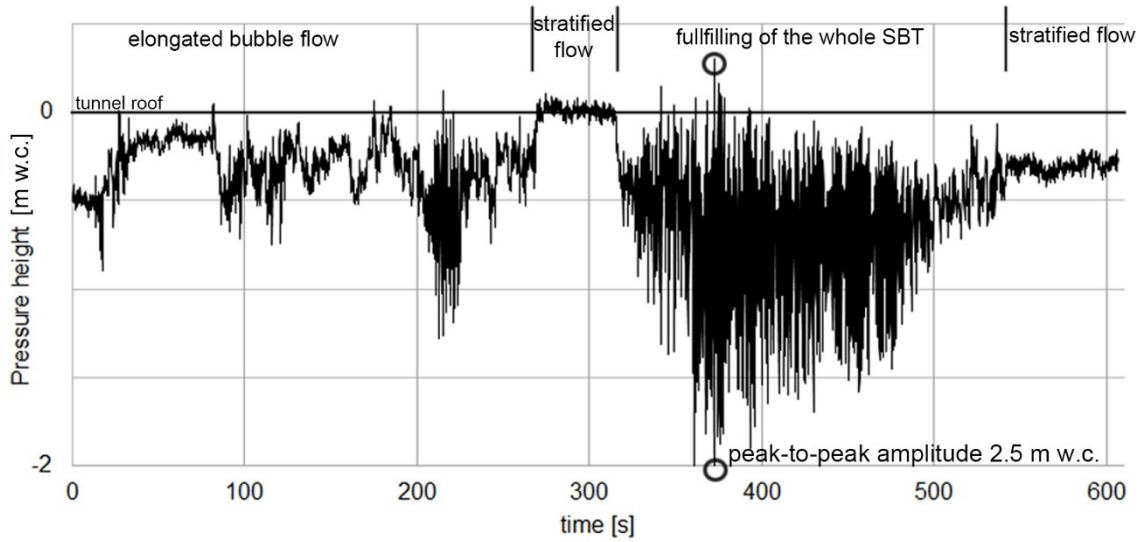

Fig. 7: Time sequence of pressure acting on the SBT roof at x = 84.6 m of the SBT in transition flow regime with Q_{SBT} = 500 m³/s (from VAW 2016).

3.4 Pressurized flow at fully opened gate

For discharges Q_{SBT} > 530 m³/s and reservoir level H_R > 755.9 m a.s.l., pressurized flow occurs in the SBT.

For the pressurized flow regime at completely opened radial gate, i.e. for drawdown flushing at moderate to large floods, negative pressure heads of up to −2.2 m w.c. (for PMF) act on the tunnel lining at the roof just in front of the transition zone at the outlet (Fig. 8) as the hydraulic gradient is steeper than the tunnel slope with simultaneous flow deceleration in the widening of the outlet cross section (Fig. 3).

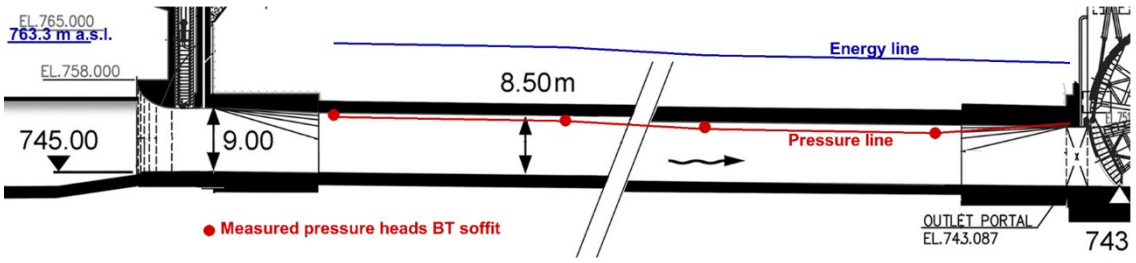

Fig. 8: Energy and pressure line in the SBT during HQ_{350} for H_R = 763.3 m a.s.l. and fully opened gate (Q_{SBT} = 830 m³/s). The pressure line is below the roof, negative pressures of up to −1.6 m w.c. act on the tunnel lining just in front of the outlet transition zone (from VAW 2016).

Time sequences of pressure measurements in pressurized flow show small pressure fluctuations lying mainly within the range of noise of the pressure transducer in the physical model and the C_p'-values of about 0.01 are typical for pressure fluctuations beneath the turbulent boundary layer of a smooth pipe flow (Narayanan 1968).

The flow velocities v, pressure heads $h_{p,mean}$, $h_{p,min}$ and $h_{p,max}$, and pressure fluctuations h_p' were measured and the dynamic pressure coefficients C_p' as well as the cavitation indices σ were derived for different load cases for drawdown flushing during flood events at the most critical measuring section with highest sub-pressures (x = 151.8 m). The pressure fluctuation parameters at the SBT roof in the other measuring sections are comparable. The maximal SBT discharge amounts to 975 m^3/s for the PMF, with a mean flow velocity of 16.9 m/s. With the mean negative pressure head of about −2.2 m w.c., a cavitation index of $\sigma \approx 0.5$ can be assessed. According to Ball (1976), a square-edged offset into the flow (positive step) at the SBT roof lining of about 1-2 mm is high enough for incipient cavitation.

4 Air entrainment and detrainment

4.1 Air entrainment rate and air transport

Depending on hydraulic and geometric boundary conditions, vortices at intakes may occur. A typical countermeasure is to design a sufficiently large submergence depth so that no air-entraining vortices of vortex type 5 and 6 (Hecker 1987) develop, as air in pressure systems may have negative effects like unsteady flow behavior, pulsations, pressure surges and gate vibrations (Gordon 1970, Kraus 1987). However, in many cases like for SBT Patrind, air-entraining vortices cannot be prevented. For the latter, even for the largest possible submergence depth, i.e. for the reservoir level at FSL, and for small SBT discharges, air-entraining vortices developed in the scale model. The vortices grew stronger with increasing Q_{SBT}. The air entrainment rate from intake vortices can be assessed based on findings of Möller *et al.* (2015), while the air transport capacity in the SBT can be assessed according to Wickenhäuser (2008) and Wickenhäuser and Kriewitz (2009). If the latter is higher than the air entrainment rate, the full air entrainment rates should be considered for the dimensioning of de-aeration devices as a countermeasure as described in 4.3.

4.2 Accumulation of air at partially lowered gate

The air entrained by vortices is collected in a coherent air core along the tunnel axis (Fig. 9). Its formation is a result of the high tangential velocity component at the spiral flow core inducing a sub-atmospheric pressure strong enough to entrain air and collect the air bubbles in its center. The coherent air core grows unstable at approx. half of the tunnel length and collapses into a chain of aligned air bubbles which start to rise toward the tunnel roof (Fig. 9). As the vortex is more strongly pronounced at prototype site a winding

line vortex with a persistent air core is likely to occur, especially along the first half of the tunnel. In the downstream tunnel half, the core is not tracked anymore in the physical scale model, illustrating the collapse of the spiral flow and the disintegration of the vortex core. Therefore, even in prototype, the air core is likely to disperse in single bubbles rising to the roof. A certain length is required for all bubbles to rise to the roof and to establish fully developed two-phase flow. For two-phase air-water SBT flow it should thus be investigated whether air bubbles (i) rise to the roof and merge to air pockets or (ii) leave the SBT unhindered below the partially-opened gate dispersed within the water phase. For case (i), air bubbles and pockets are collected in front of the gate from where they blow out periodically. This leads to pressure fluctuations on the radial gate, as described by Naudascher (1991) (Fig. 10).

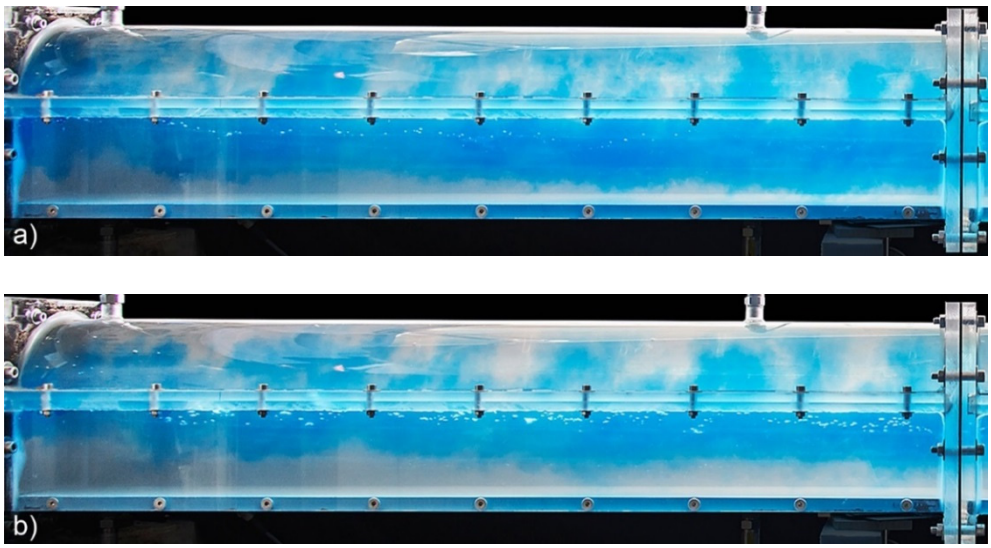

Fig. 9: Transport of air bubbles in the upstream portion of the SBT scale model for a) 300 m^3/s and 32% gate opening at FSL and b) 511 m^3/s and 60% gate opening at FSL. Dye injected into the vortex core at the free surface forms a clearly visible dye core. Air bubbles entrained by the intake vortex line up along a chain in the core of the spiral flow (flow from left to right) (from VAW 2016).

The air bubble rising length to the roof can be assessed for different water discharges using a vertical bubble rise velocity of 0.2 m/s according to Ervine and Himmo (1984) and Arch and Mayr (2006). Assuming the air core collapse to occur within one half to two-thirds of the tunnel height (4.25 m - 5.67 m for SBT Patrind) and approximately within half the tunnel length (~90 m) as observed in the Patrind scale tests, air accumulations in front of the partially-opened radial gate are expected for water discharges $Q_{SBT} < 400$ m^3/s for $H_R = 765$ m a.s.l. for the Patrind SBT. For $Q_{SBT} \geq 400$ m^3/s, flow velocities in the SBT are high enough for the air to be transported out of the short SBT before collecting at the tunnel roof. Hereby, the coherent vortex structure itself promotes keeping the air enclosed in its core until it breaks down after half the tunnel length.

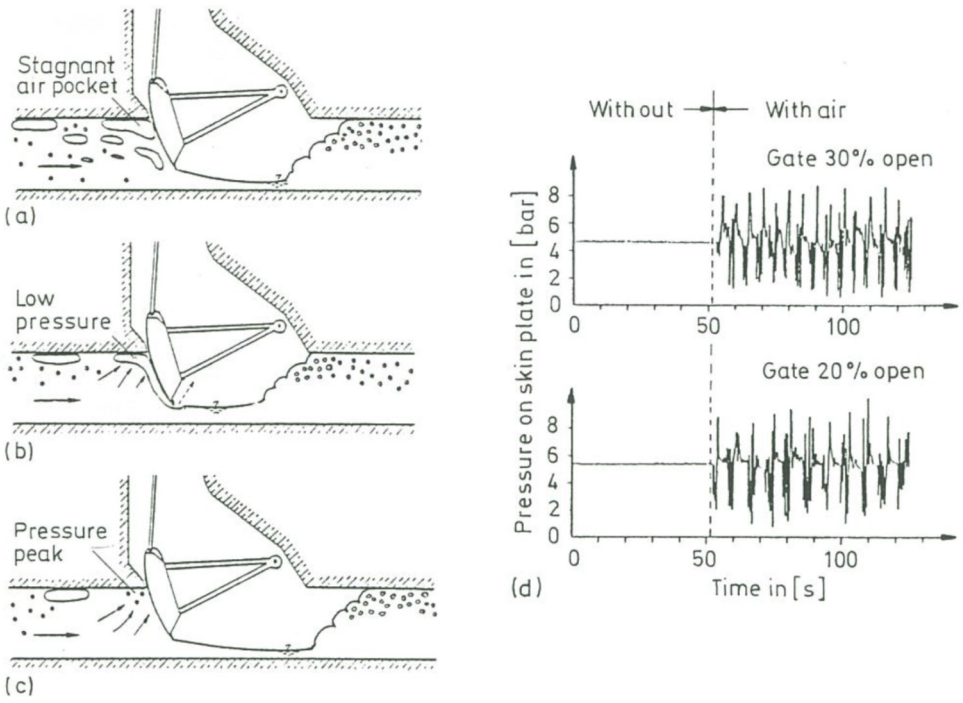

Fig. 10: (a-c) Sketch of blow-up process at 20% to 40% relative gate openings; (d) typical histograms of pressure fluctuation on upstream skin plate [Graphic after Rouvé and Traut (1980) taken from Naudascher (1991)].

4.3 Countermeasure: design of de-aeration device

As a sufficient intake submergence may be operationally unfeasible and structural elements such as anti-vortex devices (Knauss 1987) at SBT inlets are often difficult or prohibitive to construct, a de-aeration structure in front of the radial gate is necessary to avoid the pressure fluctuations mentioned above. Such a de-aeration device typically consists of a small prismatic cavity or dome above the tunnel roof from where a pipe rises to the atmosphere above ground (Wickenhäuser 2008). The required de-aeration pipe diameter d can be calculated for a given maximal water level rise h_{max} in the de-aeration pipe, depending on the local pressure height h_w above the roof and the transported air discharge Q_a according to Eq. [1] (Wickenhäuser 2008):

$$d = \sqrt{\frac{Q_a}{u_d}\left(\frac{1}{1-h_w/h_{\max}} - C_0\right)\frac{4}{\pi}} \quad \text{[m]} \qquad [1]$$

where u_d is the cross-sectionally and temporally averaged air bubble drift velocity, i.e. the relative velocity between the air phase and the surrounding fluid, and C_0 is a parameter accounting for the difference between the velocity profile and the phase distribution (i.e. air vs. fluid). For churn-slug flow in vertical pipes u_d = 0.37 m/s and C_0 = 1.31 (Wickenhäuser 2008). With h_{max} = 17.5 m, h_w = 10.7 m and Q_a = 0.031 m^3/s according to

Möller *et al.* (2015) for Q_{SBT} = 400 m^3/s, the required de-aeration pipe diameter for the Patrind SBT can be calculated with Eq. [1] to d = 0.37 m. Churn-slug or churn flow will occur in the de-aeration pipe.

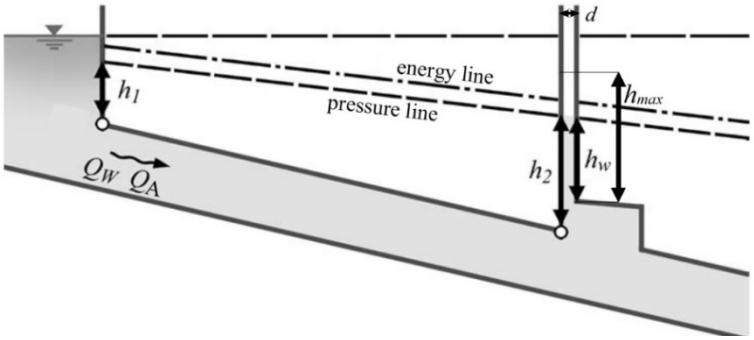

Fig. 11: Definition sketch of de-aeration pipe (from Wickenhäuser 2008).

To avoid the accumulation of larger air pockets at the tunnel roof besides an axially located de-aeration pipe, and to cover uncertainties regarding the air entrainment rates and assumptions made, the arrangement of four de-aeration pipes of 0.3-0.5 m diameter in regular intervals across the SBT roof approx. 2 m u/s of the radial gate, just d/s of the profile transition (Fig. 3), is recommended for Patrind SBT. A larger de-aeration pipe cross section also reduces the risk of geysering (Vasconcelos and Wright 2011).

5 Sediment transport

5.1 Determination of SBT transport capacity

The bedload transport capacity is usually presented in specific gravimetric form per unit width q_s^* [kg/(s·m)], in volumetric form $q_v^* = q_s^*/\rho_s$ [m^3/(s·m)] or as non-dimensional volumetric bedload transport capacity q_{vn}^* introduced by Einstein (1950)

$$q_{vn}^* = \frac{q_v^*}{\sqrt{(s-1)gD^3}} \quad [-] \qquad [2]$$

where $s = \rho_s/\rho$ = relative sediment density, with ρ_s and ρ = sediment and water density, respectively, and D = characteristic particle diameter (typically $D = D_{50}$ = median particle diameter [m]).

Numerous formulae are available for calculation of sediment transport in alluvial river systems (e.g. Meyer Peter and Müller 1948, Fernandez Luque and van Beek 1976, Parker 1990, Rickenmann 2001, Wilcock and Crowe 2003). Exemplarily, the revised version of Meyer Peter and Müller (1948) is reported here (Wong and Parker 2006):

$$q_{vn}^* = 4.93(\theta - \theta_c)^{1.6} \quad [-] \quad \text{for } 0.0004 \le S \le 0.02 \qquad [3]$$

where θ = Shields parameter calculated as $\theta = U_*^2/[(s-1)gD]$, with $U_* = (gR_hS)^{0.5}$ = friction velocity [m/s], $R_h = A/P$ = hydraulic radius [m] with A = area [m^2] and P = wetted perimeter [m], S = energy line slope [-] (subscript e) for steady but gradually-varied flow, or bed slope (subscript b) for uniform flow, and θ_c = critical Shields parameter. Meyer-Peter and Müller (1948) proposed $\theta_c = 0.047$.

For steeper slopes up to 20%, the Smart and Jäggi (1983) formula applies:

$$q_s^* = q \cdot \frac{4\rho_s}{(s-1)} \left(\frac{D_{90}}{D_{30}} \right)^{0.2} S_b^{1.6} \left(1 - \frac{\theta_c}{\theta} \right) \quad \text{[kg/(s·m)]} \quad \text{for } 0.005 \le S \le 0.20 \qquad [4]$$

where q = specific water discharge [m^3/(s·m)], D_{30} and D_{90} = characteristic diameters, at which 30% and 90% of a sample's mass are comprised of smaller particles. Note that Eq. [4] is given here for rectangular cross-section as typical for the near-bed part of SBTs where sediment transport takes place. In general form, q has to be replaced by the term ($R_b \cdot v$), where R_b = hydraulic radius of the bed-related cross-sectional flow area in a partitioned cross-section and v = mean cross-sectional flow velocity.

In general, sediment transport calculations for SBT differ from those for alluvial rivers because of low relative roughness ($k_s/h << 0.1$, with k_s = equivalent sand roughness height), non-movable bed and initially planar bed. For such conditions, only few sediment transport formulae are available such as the ones by Pedroli (1963) and Smart and Jäggi (1983). According to the former, the specific gravimetric bedload transport capacity q_s^* per unit width for planar beds is expressed by

$$q_s^* = 14.5 \cdot \frac{\tau_b^{8/5} D_m^{1/5} g^{3/5}}{\rho_s^{3/5} \nu^{1/5}} - 23.2 \rho_s \nu \quad \text{[kg/(s·m)]} \quad \text{for } 0.0004 \le S_b \le 0.02 \qquad [5]$$

where $\tau_b = \rho R_h S$ given in the unit [kg/m^2], D_m = mean particle diameter and ν = kinematic viscosity [m^2/s]. Smart and Jäggi (1983) proposed for low relative roughness

$$q_s^* = q \cdot \frac{7.35\rho_s}{(s-1)} \left(\frac{D_{90}}{D_{30}} \right)^{0.2} S_b^{1.6} \left(1 - \frac{\theta_c}{1.5\theta} \right) \quad \text{[kg/(s·m)]} \quad \text{for } 0.03 \le S_b \le 0.20 \qquad [6]$$

The choice of the critical Shields parameter θ_c for planar beds with low relative roughness is challenging. For fixed and smooth or transitionally rough beds where $k_s << D$ applies, critical values are one order of magnitude lower compared to alluvial rough river beds due to the fact that the sediment particle is totally exposed to the flow and hence its choice is not decisive for bedload calculations. For planar flume or bedrock beds, θ_c ranges from 0.001 to 0.009 (Ishibashi 1983, Chatanantavet *et al.* 2013, Inoue *et al.* 2014, Beer and Turowski 2015). The choice of $\theta_c = 0.005$ as a first guess is recommended (Auel *et al.* 2017).

If the sediment input into an SBT exceeds its transport capacity, sediment aggradations develop, steadily increasing the slope of the sediment body in the SBT until the transport capacity is high enough to sluice the incoming sediment through the SBT. For such conditions with completely covered bed the SBT resembles an alluvial river with a movable bed, so that Eq. [3] or Eq. [4] (depending on the slope) may be used to calculate the sediment transport capacity, while for SBT conditions without sediment cover along the bed Eq. [5] or Eq. [6] should be applied.

5.2 Reservoir flushing concept

The annual flushing procedure of the Patrind scheme schedules the flushing of the reservoir u/s of the cofferdam through the SBT for five days with a subsequent flushing of the natural settling basin close to the dam through the underflow spillways for one day (cf. 2.1, Fig. 2). Further, an additional flushing after large flood events might become necessary if sediment aggradations are high.

When the SBT gate is opened during the annual flushing procedure, a flushing cone forms at the tunnel inlet, resulting in a sudden, large sediment entrainment into the SBT (flushing under pressure). During the following free-flow flushing procedure the flushing cone slowly grows larger until it stabilizes and no more sediment is removed (Fig. 12). Anticipated free-surface flow flushing discharges are between 150 and 200 m^3/s. For lower discharges, the bed shear stresses in the reservoir would be insufficient to remobilize large parts of the depositions and hence the transport capacity would be low, while for larger discharges backwater effects at the SBT inlet would decrease bed shear stresses. To draw down the reservoir, typical SBT discharges are around 400 m^3/s, i.e. at incipient transition flow regime (Fig. 4).

Fig. 12: River bed morphology in the upstream reservoir reach after the flushing test with $Q_{SBT} = 200$ m^3/s showing an armouring layer. Only a flushing cone of limited size is scoured out in front of the SBT inlet. (from VAW 2016).

5.3 Sediment transport in the SBT Patrind during flushing

In the physical model, during the erosion of the flushing cone under pressurized inlet conditions a high sediment input into the SBT Patrind was observed. This resulted in a dune-like bed form sediment transport (Fig. 13). After drawdown with e.g. Q_{SBT} = 400 m^3/s, when the flushing cone has been formed, continuous transport of single grains is observed mainly along the right SBT sidewall.

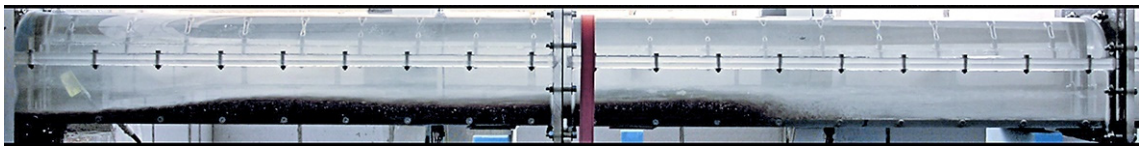

Fig. 13: Side view of the SBT during drawdown with Q_{SBT} = 400 m^3/s like for annual flushing. A dune-like bed form is transported along the tunnel during the drawdown of the reservoir with pressurized flow conditions. The sediment material comes from the deposit in front of the SBT intake which is scoured out by the flow creating a flushing cone (from VAW 2016).

In case of flushing the reservoir is drained to achieve free-flow conditions, leading to retrogressive erosion and a channel widening through the delta deposits. A high amount of sediment therefore enters the SBT, exceeding its transport capacity. The SBT is thus partially filled with sediments. The slope of the sediment body in the SBT gets steeper until the transport capacity is high enough to sluice the incoming sediment through the SBT, which is the case with a constant slope of about 4% (Fig. 14). With this boundary condition of movable bed on steep slope, 8,450 kg/s of bedload can be transported through the SBT applying Eq. [4] with θ_c = 0.047, while the transport capacity over the fixed SBT concrete bed with a slope of 1.12% amounts to about 3,700 kg/s applying Eq. [5] for Q_{SBT} = 150 m^3/s. For the upper flushing discharge limit of Q_{SBT} = 200 m^3/s, the values are 11,320 kg/s (assuming a similar slope of 4%) and 4,350 kg/s, respectively. With continuing flushing operation duration, the deposition body gradually gets flatter and is finally washed out with decreasing sediment input into the SBT.

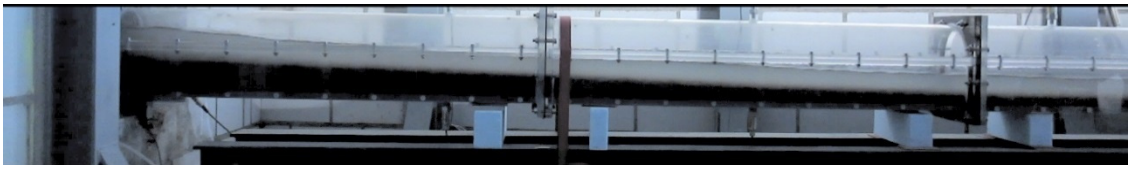

Fig. 14: Side view on the SBT free-surface flow with Q_{SBT} = 150 m^3/s during drawdown for the additional flushing after large sediment deposits have been formed in the u/s reservoir. The flushing efficiency in the reservoir and sediment transport in the SBT are high at the beginning of the flushing test. The sediment aggradation in the SBT reaches a constant slope of about 4%. At the end of the test, the SBT is cleared from these deposits. Although the deposits in the SBT are high, free-flow conditions prevail (from VAW 2016).

6 Conclusions

As exemplified by the SBT Patrind case study presented herein, the following general conclusions for SBTs with gated d/s control may be drawn:

The flow regimes are threefold depending on discharge and gate opening: (i) free-surface flow, (ii) transition flow with transient transport of air bubbles and (iii) pressurized flow. With both the transitional and pressurized regimes undesirable air entrainment, air transport and air accumulations may occur and become critical.

A large intake vortex may occur directly in front of the SBT inlet structure under pressurized flow conditions, which leads to air entrainment for all gate openings during normal operation and simultaneous sluicing through the SBT at certain reservoir levels. The vortex leads to spiral flow inside the tunnel, which affects the air and sediment transport. Entrained air accumulating in front of the partially opened d/s gate may lead to an inadmissible impact on the gate. To avoid air-entraining vortices, either sufficient submergence should be considered or an anti-vortex device should be implemented at the SBT inlet structure. Alternatively, the entrained air can be released with the installation of de-aeration pipes located slightly u/s of the outlet gate. However, it should be accounted for that the release of trapped air out of the de-aeration device occurs with high velocities, which might imply danger to object or people in the vicinity. If the installation of a de-aeration device is the only viable way, hydraulic model investigations are highly recommended because available design criteria for de-aeration devices were developed for headrace tunnels with moderate flow velocities, and are not directly applicable to high-speed SBT flows.

During pressurized flow conditions at large discharges a drop of the pressure line below the upstream tunnel roof occurs in case of profile transition to a larger cross sectional area at the outlet section, leading to negative pressure heads. These negative pressures in the d/s part of the tunnel as well as dynamic loads during the transition regime due to the consequent air entrainment should be regarded as a design requirement.

The operation with high velocities and negative pressure heads leads to incipient cavitation in case of irregularities in the SBT lining. An offset into the flow at the SBT roof lining of about 1-2 mm may suffice for incipient cavitation at large discharges. An appropriate design of the joints is therefore recommended. At the SBT bottom, abrasion damages might promote the danger of incipient cavitation. Regular inspections after SBT operation will be necessary to assess abrasion and cavitation damages.

Despite the typically high transport capacity of hydraulically smooth or transitionally rough SBTs, temporary and local aggradations cannot be excluded within the tunnel during high sediment input from deposits at the tunnel inlet. The depositions must not lead to flow choking. The critical phase is the first opening after a relatively long period with significant sediment depositions at the SBT inlet. In order to limit these aggradations

at the inlet, they should therefore be monitored and regularly flushed out under pressurized flow conditions before reaching the inlet crown.

By regulating an SBT at the inlet structure, free-flow conditions prevail in the tunnel and the discussed issues such as unfavourable air entrainment, air accumulation at gates and negative pressures on the tunnel lining can be avoided. Therefore, downstream-controlled SBTs should only be selected if other design options fail.

Acknowledgement

The authors are thankful to SAMAN Corp., South Korea, for the mandate to carry out the hydraulic scale modeling on the Patrind hydropower project including its SBT. The study was embedded into the framework of the Swiss Competence Center for Energy Research – Supply of Electricity (SCCER-SoE).

References

Alam, S., Roca, M., Petkovsek, G., Kim, S.-H., Shin, K. (2015). Use of the Patrind hydroelectric project forebay area as a "natural" de-sander, *Proc. Hydro 2015 Conference*, Bordeaux, France.

Arch, A., Mayr, D. (2006). De-aeration of air-water flows in the tailwater channels of Pelton turbines, *International Journal of Hydropower & Dams*, 13(2), 106–110.

Auel, C. (2014). Flow characteristics, particle motion and invert abrasion in sediment bypass tunnels. *VAW-Mitteilung* 229, R.M. Boes, ed., Laboratory of Hydraulics, Hydrology and Glaciology, ETH Zurich, Switzerland.

Auel, C., & Boes, R.M. (2011). Sediment bypass tunnel design – review and outlook. Proc. ICOLD Symposium „Dams under changing challenges" (A.J. Schleiss & R.M. Boes, eds.), 79th Annual Meeting, Lucerne. *Taylor & Francis*, London: 403-412.

Auel, C., Albayrak, I., Sumi, T., Boes, R.M. (2017). Sediment transport in high-speed flows over a fixed bed: 1. Particle dynamics. *Earth Surface Processes and Landforms*, DOI: 10.1002/esp.4128.

Ball, J.W. (1976). Cavitation from surface irregularities in high velocity. *Journal of the Hydraulics Division*, ASCE, Vol. 102, No. HY9, 1283-1297

Beck, C., Lutz, N., Lais, A., Vetsch, D., Boes, R. M. (2016). Patrind Hydropower Project, Pakistan Physical model investigations on the optimization of the sediment management concept. *Proc. Hydro 2016 Conference*, Montreux, Switzerland.

Beer, A. R., Turowski, J. M. (2015). Bedload transport controls bedrock erosion under sediment-starved conditions. *Earth Surface Dynamics 3*: 291–309. DOI: 10.5194/esurf-3-291-2015.

Carlioz, P., Peloutier, V. (2014). Implementing a sediment transit gate at Rizzanese dam. *Proc. Intl., ICOLD Sympoium on Dams in a Global Environmental Challenges*, Bali, Indonesia, Abstract number 346.

Chatanantavet, P., Whipple, K. X., Adams, M. A., Lamb, M. P. (2013). Experimental study on coarse grain saltation dynamics in bedrock channels. *Journal of Geophysical Research: Earth Surface.* 118(2): 1161–1176. DOI: 10.1002/jgrf.20053.

Einstein, H.A. (1950). The bed-load function for sediment transportation in open channel flows. *United States Department of Agriculture*, Washington D.C., USA.

Ervine, D.A., Himmo, S.K. (1984). Modelling the behaviour of air pockets in closed conduit hydraulic systems. *IAHR, Symposium on scale effects in modelling hydraulic structures*, Esslingen: 4.15.

Fernandez Luque, R., van Beek, R. (1976). Erosion and transport of bed-load sediment. *Journal of Hydraulic Research* 14(2): 127–144.

Gordon, J. L. (1970). Vortices at intakes. *Water Power*, 22(4), 137-138.

Hagmann, M., Albayrak, I., Boes, R.M., Auel, C., Sumi, T. (2016). Reviewing research and experience on sediment bypass tunnels. *Hydropower & Dams* 23(1): 54-58.

Hecker, G. E. (1987). Fundamentals of vortex intake flow, swirling flow problems at intakes. *IAHR hydraulic structures design manual, Vol. 1*, Balkema, Rotterdam, Netherlands, 13–38.

Inoue, T., Izumi, N., Shimizu, Y., Parker, G. (2014). Interaction among alluvial cover, bed roughness, and incision rate in purely bedrock and alluvial-bedrock channel. *Journal of Geophysical Research: Earth Surface,* 119(10): 2123−2146. DOI: 10.1002/2014JF003133.

Ishibashi, T. (1983). Hydraulic study on protection for erosion of sediment flush equipment of dams. *Civil Society Proc.* 334(6): 103–112 (in Japanese).

Knauss, J. (1987). Swirling flow problems at intakes. *IAHR Hydraulic Structures Manual* 1. Balkema, Rotterdam, The Netherlands, 13-38

Laperrousaz, E., Carlioz, P. (2015). Rizzanese sediment bypass tunnel. Proc. 1st Intl. Workshop on Sediment Bypass Tunnels Zürich. *VAW-Mitteilung* 232: 95-100, R.M. Boes, ed., Laboratory of Hydraulics, Hydrology and Glaciology, ETH Zurich, Switzerland.

Meyer-Peter, E., Müller, R. (1948). Formulas for bedload transport. *Proc. 2nd Meeting Int. Association of Hydraulic Structures Research*, Stockholm, Sweden: 39–64.

Möller, G., Detert, M. & Boes, R.M. (2015). Vortex-induced air entrainment rate at intakes. *Journal of Hydraulic Engineering* 141(11), 04015126.

Narayanan, R., Reynolds, A.J. (1968). Pressure fluctuations in reattaching flow. *Journal of the Hydraulic Division*, Proceedings of the ASCE, Vol. 94, No. HY6, 1383-1398

Naudascher, E. (1991). Hydrodynamic forces, *IAHR Hydraulic Structures Design Manual* 3. Balkema, Rotterdam, The Netherlands.

Parker, G. (1990). Surface-based bedload transport relation for gravel rivers. *Journal of Hydraulic Research* 28(4): 417−436. DOI: 10.1080/00221689009499058.

Pedroli, R. (1963). Trasporto di material solido in canali a fondo fisso e liscio ('Transport of solid material in channels on a fixed and smooth bed'). *Mitteilung des Eidg. Amtes für Wasserwirtschaft* 43, Eidgenössisches Verkehrs- und Energiewirtschaftsdepartement, Switzerland (in Italian).

Rickenmann, D. (2001). Comparison of bed load transport in torrents and gravel bed streams. *Water Resources Research* 37(12): 3295−3305. DOI: 10.1029/2001WR000319.

Rouvé, G., Traut, F.J. (1980). Vibrations due to two-phase flow below a Tainter gate. *Practical experiences with flow-induced vibrations*, E.Naudascher & E.Rockwell (eds.), Springer, p. 461

Smart, G. M, Jäggi, M. N. R. (1983). Sediment transport on steep slopes. *VAW-Mitteilung* 64, D. Vischer, ed., Laboratory of Hydraulics, Hydrology and Glaciology, ETH Zurich, Switzerland.

Vasconcelos, J. G. and Wright, S. J. (2011). Geysering generated by large air pockets released through water-filled ventilation shafts. *Journal of Hydraulic Engineering*, 137(5), 543-555.

VAW (2016). Patrind hydropower project: Physical model investigation of the weir site – Hydraulic and sedimentological tests. *VAW-Report* 4325, Laboratory of Hydraulics, Hydrology and Glaciology, ETH Zurich, Switzerland (unpublished).

Wickenhäuser, M. (2008). Zweiphasenströmung in Entlüftungssystemen von Druckstollen ('Two-phase flow in de-aeration systems of pressurized tunnels'). *VAW-Mitteilung* 205, H.-E. Minor, ed., Laboratory of Hydraulics, Hydrology and Glaciology, ETH Zurich, Switzerland. (in German).

Wickenhäuser, M., Kriewitz, C.R. (2009). Air-Water Flow in Downward Inclined Large Pipes. *Proc. 33rd IAHR Congress: Water Engineering for a Sustainable Environment*. IAHR, Vancouver, 5354-5361.

Wilcock, P. R., Crowe, J. C. (2003). Surface-based transport model for mixed-size sediment. *Journal of Hydraulic Engineering* ASCE 129(2): 120−128. DOI: 10.1061/(ASCE)0733-9429(2003)129:2(120).

Wong, M., Parker, G. (2006). Reanalysis and correction of bed-load relation of Meyer-Peter and Müller using their own database. *Journal of Hydraulic Engineering* 132(1), 1159–1168.

Authors

Robert Michael Boes (corresponding Author)
Claudia Beck
Nicola Lutz
Adriano Lais
Ismail Albayrak
Laboratory of Hydraulics, Hydrology and Glaciology (VAW), ETH Zurich, Switzerland
Email: boes@vaw.baug.ethz.ch